Atomic motions in an unusual molecular semiconductor: NaSn

Ronald Dean Stoddard, Mark S. Conradi, and A. F. McDowell
Department of Physics-1105, Washington University, One Brookings Drive, St. Louis, Missouri 63130

Marie-Louise Saboungi and David Long Price
Argonne National Laboratory, Argonne, Illinois 60439
(Received 17 April 1995)

Recent investigations of the compound NaSn (1:1) have indicated that both fast conduction of Na^+ cations and rapid reorientations of $(Sn_4)^{4-}$ anions are present in the high-temperature solid phase, α-NaSn. We have used ^{23}Na and ^{119}Sn nuclear magnetic resonance to separately monitor the motions of Na and Sn in the low-temperature ordered solid phase, β-NaSn, where the correlation times of the motions are much longer. The Na^+ motions are evident in T_1, $T_{1\rho}$, T_2, and T_2^* (linewidth) ^{23}Na data at magnetic fields of 8.0 and 2.0 T. The Na motions are described by a single time constant with thermal activation parameters $E_a/k_B = 9700$ K and $\omega_D(\infty) = 1.7 \times 10^{14}$ s^{-1}. Sn motions are evident in T_2, line shape, and stimulated echo data taken at 8.0 T. ^{119}Sn stimulated echo data unequivocally show the Sn motion to be reorientations of Sn_4 tetrahedra; any diffusion of Sn between tetrahedra is much slower. The combined T_2 and stimulated echo data for ^{119}Sn demonstrate that the Sn_4 reorientations are thermally activated with $E_a/k_B = 13\,800$ K and $\omega_R(\infty) = 2.3 \times 10^{15}$ s^{-1}. The temperature dependence of the ^{119}Sn T_1 fits an activation energy of 7000 K; the Sn T_1 is believed to be due to thermally-activated charge carriers.

I. INTRODUCTION

The low-temperature solid phase of NaSn (β-NaSn) has a tetragonal structure with the space group D_{4h}^{20}-I4/*acd* and is isomorphic with all other 1:1 compounds of an alkali metal with tin or lead.[1] In NaSn, the large difference in the electronegativities of Na and Sn leads to the formal transfer of an electron from Na to Sn. The Sn^- ions are bound into stable $(Sn_4)^{4-}$ tetrahedra, which are isoelectronic with the P_4 tetrahedra in white phosphorus,[2] and these Sn_4 molecular units lie on a body-centered tetragonal lattice.[1] The Sn_4 tetrahedra are separated by Na^+ ions which lie on two types of sites, denoted Na(1) and Na(2). The Na(1) sites lie opposite the face centers of the Sn_4 tetrahedra, forming larger tetrahedra directed opposite the Sn_4 units. The Na(2) sites form squares in the (*a*-*b*) plane which are concentric with the Sn_4 tetrahedra. Each Na^+ ion is shared between two Sn_4 tetrahedra. The chemical rationalization for this structure is that it allows all of the atoms to have closed outer shells, leading to ionic bonding of the Na^+ ions to the $(Sn_4)^{4-}$ tetrahedra and covalent bonding within the Sn_4 units.[3] This type of bonding, characteristic of Zintl alloys,[4] leads to behavior which is very different from that naively expected of an alloy of two metals. The high electrical resistivity of NaSn shows that this is a semiconductor, not a metal.[5]

In 1928, Hume-Rothery found that the stoichiometric compound NaSn undergoes a polymorphic phase transition from β-NaSn (stable below 483 °C) to α-NaSn (stable from 483 °C to the congruent melting point at 578 °C).[6] More recent studies of NaSn have confirmed the existence of this phase transition and have investigated the properties of the transition more carefully.[5,7] In Ref. 7, the enthalpy vs temperature for NaSn is presented; both the α-β and the solid-liquid transitions for NaSn are evident as nearly vertical risers (discontinuities in H vs T). Surprisingly, the entropy change for the α-β transition, $\Delta S_{\alpha-\beta} = 4.95$ J mol^{-1} K^{-1}, is nearly as large as for melting, $\Delta S_{\rm melt} = 8.48$ J mol^{-1} K^{-1}. Another interesting aspect is that the lattice of α-NaSn has *lower* symmetry than β-NaSn. The structure of α-NaSn is not known in detail, but the lattice is triclinic.[5]

Neutron scattering experiments performed on liquid NaSn (1:1 stoichiometry) indicate that Sn_4 tetrahedra survive into the melt, suggesting that the Sn_4 units are also present in α-NaSn as well.[8] Electrical resistivity measurements on melts of $Na_{1-x}Sn_x$ show a strong maximum[9] near $x = 0.43$, giving further evidence that Zintl (closed-shell) bonding is present in liquid NaSn and, undoubtedly, α-NaSn.

The occurrence of α-NaSn just below the melting temperature and the large α-β transition entropy suggest α-NaSn is dynamically disordered. Because Sn_4 units are present, α-NaSn may be an orientationally disordered (rotor) phase. The presence of the Na^+ ions suggests α-NaSn may be a superionic conductor, that is, the Na may be translationally delocalized. In fact, neutron scattering finds[5] that *both* Sn_4 rotations and Na diffusion occur in α-NaSn. The single phase transition to the disordered phase and the single time constant for the motions suggest that the two motions are highly coupled, one possibly driving the other. A paddlewheel model of the motion, similar to that described[10] for Li_2SO_4, has been proposed.[5]

0163-1829/95/52(19)/13998(8)/$06.00

The focus of our work is β-NaSn, where correlation times are long enough that NMR provides detailed insight. We believe motions in β-NaSn include precursors to the motions of the disordered phase, α-NaSn. In particular, ^{119}Sn NMR monitors reorientations of Sn_4 subunits and ^{23}Na NMR is sensitive to translational diffusion of Na^+ cations.

II. EXPERIMENT

The NaSn samples used here are from a batch prepared at Argonne and used in previous experiments.[5,7] The powder samples were transported in sealed Pyrex tubes under an inert atmosphere, transferred in a nitrogen glovebox to quartz tubes, evacuated and backfilled with argon, and then sealed. In order to use a horizontal solenoidal rf coil for the high-field experiments, the quartz tubes were sealed short ($\sim$ 2 cm) using a massive copper flame shield to protect the sample.

The NMR experiments were performed with a superheterodyne pulsed spectrometer. For the high-field experiments an 8.0 T superconducting magnet was used. The resonance frequencies of ^{23}Na and ^{119}Sn, the nuclei of interest, are 90.11 MHz and 126.86 MHz, respectively. For the low-field (2.0 T) ^{23}Na work at 22.49 MHz a water cooled electromagnet equipped with ^{19}F field regulation was used.

Separate high-temperature furnaces were used for the low-field and high-field NMR measurements. Sheathed thermocouple wire (type E, nonmagnetic) serves as heater resistance windings. The thermocouple wires are naturally bifilar, providing nearly noninductive heaters. The heaters are insulated with ceramic blankets to improve temperature homogeneity. The high-field furnace fits into a water jacket to prevent heat transfer to the magnet, while air cooling at the base is sufficient for the low-field furnace. The NMR probes are transmission line designs,[11,12] enabling the use of conventional air variable capacitors for tuning and matching the resonant circuit. The capacitors are mounted in an aluminum box outside the magnet, at room temperature. Each NMR probe is equipped with a sheathed type-E thermocouple for monitoring sample temperature. Both furnaces are evacuated and backfilled with argon to prevent oxidation of the copper components of the probes.

For the high-field probe, the effective $\pi/2$ pulse times for ^{23}Na were 9 μs (this refers to nutation of the central transition only, a true nutational angle[13] of $\pi/4$) using a 50 W rf amplifier. For ^{119}Sn NMR, 600 W resulted in 9 μs $\pi/2$ pulses. In the low-field probe, the $\pi/2$ pulse time for ^{23}Na was 3.5 μs with 25 W of power.

III. RESULTS AND DISCUSSION

A. ^{23}Na spectra

For a correct understanding of relaxation of a quadrupolar spin such as ^{23}Na, it is crucial to determine the approximate magnitude of the static quadrupole interaction and whether the rf pulses perturb all $2I$ transitions or only the central transition. Thus the ^{23}Na spectrum of β-NaSn was examined.

In the case of a spin-3/2 nucleus, irradiation of only the central transition ($m = -1/2 \Longleftrightarrow 1/2$) results in an effective $\pi/2$ pulse length which is half as long as the $\pi/2$ pulse in the case of irradiation of all three transitions (as in a liquid).[13] We experimentally determined the length of an effective $\pi/2$ pulse by adjusting the pulse width for the largest amplitude free induction decay (FID). Using this method, the length of an effective $\pi/2$ pulse for ^{23}Na in NaSn at room temperature was found to be 0.7 times the length of a $\pi/2$ pulse for ^{23}Na in an aqueous solution of sodium acetate in the same probe. This demonstrates that we are irradiating primarily the central transition in NaSn. We believe that the observed factor is larger than 0.5 because of rf losses in the weakly conducting NaSn sample. To verify that we were only observing the central transition, the ^{23}Na *satellite* spectrum ($m = -3/2 \Longleftrightarrow -1/2$ and $1/2 \Longleftrightarrow 3/2$) was measured at room temperature with a stepped-frequency, spin echo experiment, the results of which are shown in Fig. 1. This experiment was performed by stepping the spectrometer frequency through the broad ^{23}Na satellite lines and irradiating all of the spins within the rf pulse bandwidth (7 μs pulses were used). The amplitude of the spin echo at each frequency was measured to determine the relative number of spins within the bandwidth, and then plotted versus frequency to yield a low-resolution ($\sim$ 100 kHz per point) ^{23}Na spectrum. The satellite spectrum depends on the strength ν_Q and asymmetry η ($0 \leq \eta \leq 1$) of the electric field gradient (EFG) interaction tensor. For $\nu_Q \ll \nu_0$ (ν_0 is the Larmor precession frequency) as applies here, first-order perturbation theory can be used to calculate the spectrum.[14] The overall spectral width is $2\nu_Q$; from Fig. 1 one estimates $\nu_Q \sim 750$ kHz. The breadth of the satellite spectrum of Fig. 1 shows that the rf pulses used

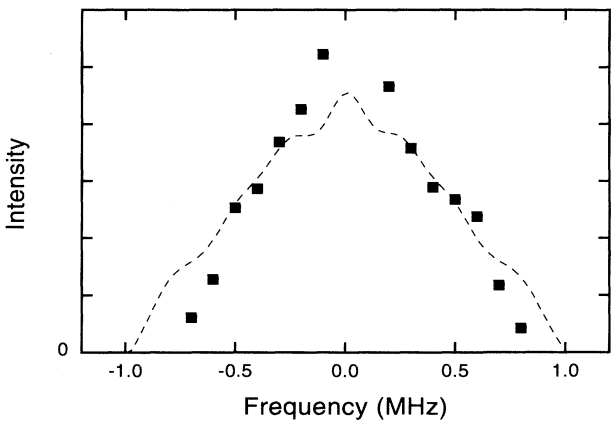

FIG. 1. The low-resolution ^{23}Na satellite spectrum, shown as solid squares. The dashed curve is a sum of two simulated spin-3/2 powder patterns with $\eta = 0.4$, $\nu_Q = 827$ kHz and $\eta = 1.0$, $\nu_Q = 900$ kHz. The simulated spectrum has been convoluted with a Gaussian of width 150 kHz in order to compare to the low-resolution experiment. The central transition is absent from the simulated spectrum.

in the central transition experiments do in fact nutate primarily the central transition only. For an EFG of axial symmetry ($\eta = 0$), strong cusps ($\omega^{-1/2}$ divergences) are expected. The relatively featureless spectrum of Fig. 1 rules out the $\eta = 0$ case. Instead, for $\eta \neq 0$, weaker logarithmic singularities are predicted, symmetrically about the Larmor frequency with splitting $\nu_Q(1\text{-}\eta)$. The logarithmic divergences are barely apparent as shoulders in the low-resolution (100 kHz per point) spectrum of Fig. 1.

The field dependence of the central transition width shows that the observed line is broadened by second-order quadrupole effects. The width of a central transition dominated by second-order quadrupole broadening[14] is proportional to ν_Q^2/ν_0; thus inversely proportional to ν_0. For spectra dominated by chemical shift anisotropy broadening, the linewidth is linear in ν_0 and for spectra dominated by dipolar broadening the linewidth is independent[15] of ν_0. Room temperature ^{23}Na central transition line shapes at 2.0 and 8.0 T are shown in Fig. 2. The 2.0 T sodium spectrum has a width (35.5 kHz) nearly three times as large as the sodium linewidth (12.9 kHz) at 8.0 T. This indicates that our observed line shape is a central transition broadened primarily by the quadrupole interaction in second order. The discrepancy between the observed (3) and expected (4) ratio of the linewidths is due to the field independent contribution from the dipolar interaction; a reasonable dipolar broadening of 2–3 kHz full width at half maximum (FWHM) accounts for the effect. The high-field spectrum shows much less structure than the spectrum at low field because of the dipolar broadening. The T_2^* data in Fig. 3 show clearly that the room temperature spectrum is in the rigid-lattice limit (no motion) so that dipolar broadening is expected.

Dr. J. Haase of Leipzig generously provided us with a set of theoretical second-order quadrupole broadened powder pattern spectra for the central transition of a spin-3/2 nucleus.[16] The spectra were for values of η between 0 and 1, in steps of 0.1. Using these theoretical line shapes we fitted the experimental central transition spectrum at 2.0 T to obtain values for η and ν_Q. The spectrum could not be fitted with a single powder pattern, not surprising given the existence of two chemically inequivalent Na^+ sites in the x-ray-derived structure.[1] Figure 2 shows a reasonable fit (dashed curve) using a superposition of two theoretical powder patterns of equal intensities (areas), with the parameters $\eta = 0.4$, $\nu_Q = 827$ kHz and $\eta = 1.0$, $\nu_Q = 900$ kHz. The powder patterns were convoluted with a Gaussian of width 1.5 kHz FWHM to account for dipolar broadening. Figure 1 shows a simulation of the expected first-order satellite spectrum as a dashed curve. The simulated spectrum has been broadened by convolution with a Gaussian of width 150 kHz FWHM, for comparison with the low-resolution experimental spectrum. The agreement with the overall width is good, confirming the values of ν_Q derived from the central transition spectrum. The parameters determined from the ^{23}Na spectra are used below to interpret the relaxation data in terms of Na motion.

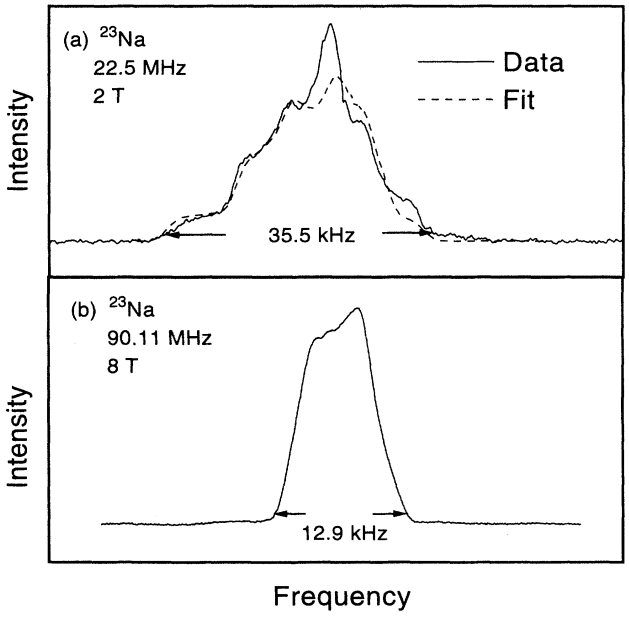

FIG. 2. ^{23}Na NMR spectra: (a) low-field (22.5 MHz) and (b) high-field (90.11 MHz). The structure in the low-field spectrum indicates that this is the ^{23}Na central transition, broadened by second-order quadrupole effects. The dashed line is a fit to the data of two superimposed second-order quadrupole powder patterns with the parameters $\eta = 0.4$, $\nu_Q = 827$ kHz and $\eta = 1.0$, $\nu_Q = 900$ kHz.

B. Na motion

The second-order quadrupole and dipole interactions will be modulated by motion of Na atoms.[15] The electric field gradient tensor is different on the two kinds of Na sites; further, the tensor principal axes are *oriented* differently, even on Na sites of the same type. Thus, Na motion will result in steplike changes in Na NMR frequency. Motional modulation of the line broadening interactions is

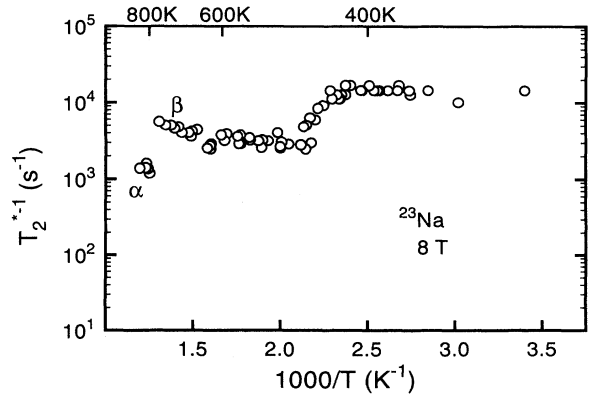

FIG. 3. High-field ^{23}Na $(T_2^*)^{-1}$ from central transition FID's (essentially the linewidth) as a function of reciprocal temperature. The observed line narrowing above 420 K implies Na motion with $\omega_D = 2 \times 10^4$ s^{-1} at 420 K.

apparent in $(T_2^*)^{-1}$, the decay rate of the FID, and T_2^{-1}, the decay rate of the spin-echo envelope. $(T_2^*)^{-1}$ data at 8.0 T (90.11 MHz) show that the central transition resonance line narrows by a factor of 8, beginning at 420 K (Fig. 3). At the onset of line narrowing, the hopping rate ω_D is approximately equal to the static central transition linewidth;[17] thus $\omega_D \sim 2\times10^4$ s^{-1} at 420 K. T_2^{-1} data at 2.0 T (22.49 MHz), where the second-order quadrupole interaction dominates, are shown in Fig. 4. There is a distinct peak in T_2^{-1} at 430 K which is due to motional broadening. For $\omega_D \ll \Delta\omega_{\rm RL}$ (the rigid-lattice width of the inhomogeneously broadened line), the strong collision theory applies.[15,18] That is, an atomic jump of a given spin during the spin-echo sequence causes that spin to be fully dephased (phase error $\Delta\phi \gg 1$) and its contribution to the echo amplitude to become zero. Thus, to within a numerical factor of order 1,

$$T_2^{-1} = \omega_D + (T_2)^{-1}_{\rm DIP} \tag{1}$$

where $(T_2)^{-1}_{\rm DIP}$ describes spin-spin decay from other mechanisms (e.g., like-spin dipolar). For $\omega_D \gg \Delta\omega_{\rm RL}$, the theory of line narrowing applies[15] and

$$T_2^{-1} = \frac{M_2}{\omega_D} + (T_2)^{-1}_{\rm DIP} = \frac{(\Delta\omega_{\rm RL})^2}{\omega_D} + (T_2)^{-1}_{\rm DIP}, \tag{2}$$

to within a factor of order unity. The motional broadening peak occurs in the intermediate region ($\omega_D \simeq \Delta\omega_{\rm RL}$) between the strong collision limit and the line narrowing limit. In this region the expressions for T_2^{-1} in the strong collision limit and the line narrowing limit are both approximately correct. Setting $\omega_D = \Delta\omega_{\rm RL}$, both expressions agree and yield the maximum spin-dephasing rate $(T_2^{-1})_{\rm max}$:

$$(T_2^{-1})_{\rm max} = \Delta\omega_{\rm RL} + (T_2)^{-1}_{\rm DIP}. \tag{3}$$

The observed value for the maximum relaxation rate, $(T_2^{-1})_{\rm max} = 2\times10^4$ s^{-1}, is in reasonable agreement with the predicted value for the maximum rate, $\Delta\omega_{\rm RL} = M_2^{1/2} = 4.6\times10^4$ s^{-1} [here $(T_2)^{-1}_{\rm DIP}$ is negligible]. Thus ω_D is approximately equal to 4×10^4 s^{-1} at 430 K. The minimum in T_2^{-1} near 500 K reflects competition between T_1^{-1} and T_2^{-1} in the line narrowing regime.[19]

Figure 5 shows ^{23}Na T_1^{-1} data for two fields; 8.0 and 2.0 T. The high-field β-NaSn data show an activated T_1^{-1} mechanism with an activation energy of 9700 K. The room temperature T_1^{-1} increased after the samples had been at high temperatures a prolonged time, but T_1^{-1} at high temperatures remained the same. We believe the room temperature relaxation is due to impurities leading to electrons or holes or fixed paramagnetic relaxation centers. For a spin-3/2 nucleus for which T_1^{-1} relaxation is due to motional modulation of the quadrupolar interaction, Abragam[20] gives the relaxation rate

$$T_1^{-1} = \frac{1}{10}(\omega_Q)^2\left(1+\frac{\eta^2}{3}\right)\left(\frac{2\tau_D}{1+\omega_0^2\tau_D^2} + \frac{8\tau_D}{1+4\omega_0^2\tau_D^2}\right) \tag{4}$$

where ω_Q is the quadrupolar coupling constant, η is the asymmetry parameter of the quadrupolar interaction tensor, and $\tau_D = 1/\omega_D$. A maximum in T_1^{-1} is expected for $\omega_0\tau_D = 0.6$ but is not seen in the high-field data. This may occur because ω_D remains smaller than ω_0 (about 10^9 s^{-1}) even at the highest temperatures in β-NaSn. To test this, we measured T_1^{-1} at a lower field (2.0 T). In Fig. 5, the low-field T_1^{-1} data reveal a thermally activated relaxation mechanism with an activation energy of 9700 K and a peak at 720 K, just below the α-β transition. Using the relation $\omega_0\tau_D = 0.6$ at the T_1^{-1} maximum, we determine that $\omega_D = 2.5\times10^8$ s^{-1} at 720 K. For $\omega_0\tau_D = 0.6$, Eq. (4) reduces to

$$(T_1^{-1})_{\rm max} \sim (0.285)\left(1+\frac{\eta^2}{3}\right)\left(\frac{\omega_Q^2}{\omega_0}\right). \tag{5}$$

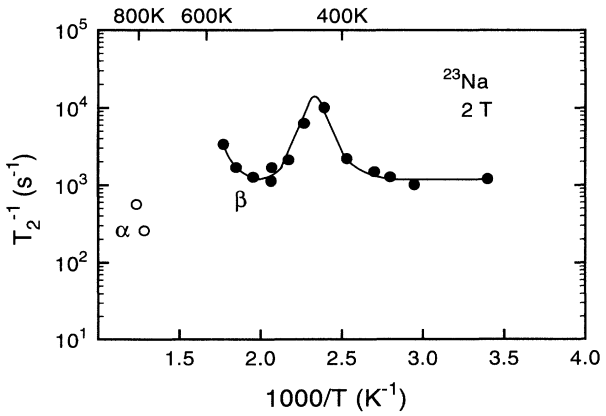

FIG. 4. Low-field ^{23}Na spin-spin relaxation rate T_2^{-1} from spin echoes as a function of reciprocal temperature. The peak in T_2^{-1} at 430 K is a motional broadening peak resulting from Na jumping. The curve is a guide for the eyes.

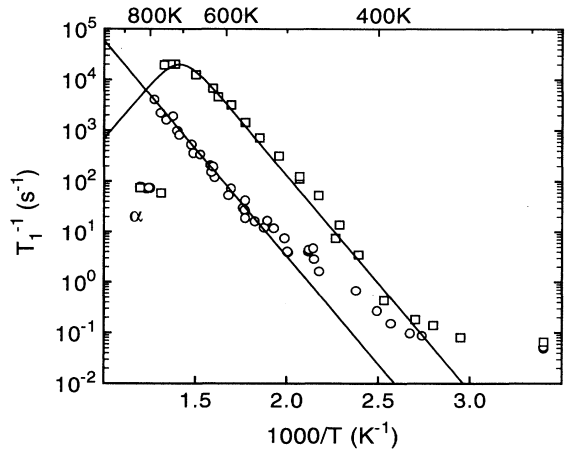

FIG. 5. ^{23}Na spin-lattice relaxation rates T_1^{-1} as a function of reciprocal temperature. High-field data are shown as circles, low-field data as squares. Both sets of data show a thermally activated relaxation mechanism with an activation energy of $E_a/k_B = 9700$ K. From the peak in the low-field data it is determined that $\omega_D = 2.5\times10^8$ s^{-1} at 720 K.

In order to calculate a value for $(T_1^{-1})_{max}$ we averaged over the two Na sites ($\eta = 0.4$, $\nu_Q = 827$ kHz; $\eta = 1.0$, $\nu_Q = 900$ kHz). Using this method we predict that $(T_1^{-1})_{max} \sim 7.2 \times 10^4$ s^{-1}. This is in tolerable agreement with the observed value, $(T_1^{-1})_{max} = 2 \times 10^4$ s^{-1}, confirming that this is a quadrupolar T_1^{-1} maximum. We note that the predicted maximum rates T_1^{-1} and T_2^{-1} are both of order ω_Q^2/ω_0, a general feature of central transition resonances.[19]

In the limit $\omega_0\tau_D \gg 1$, Eq. (4) reduces to

$$T_1^{-1} = \frac{2}{5}\frac{\omega_Q^2}{\tau_D}\left(1+\frac{\eta^2}{3}\right)\frac{1}{\omega_0^2}. \quad (6)$$

Therefore, on the cold side of the T_1^{-1} maximum, the ratio of the relaxation rates at the two frequencies should be 16 due to the ω_0^{-2} dependence of T_1^{-1}. The observed factor is 45. The discrepancy is due to a substantial temperature gradient (20–30 K) between the sample and the thermocouple in the high-frequency measurements (Fig. 5). The temperature offset is also evident in Fig. 5 from the step changes in T_1^{-1} at $T_{\alpha\beta}$ at each frequency. The step in the high-frequency data appears some 30 K hotter than in the low-frequency data. Shifting the high-frequency data by 30 K results in the expected factor of 16 frequency dependence.

High-field $T_{1\rho}^{-1}$ data for ^{23}Na are shown in Fig. 6. At low temperatures, $T_{1\rho}^{-1}$ reflects modulation of the dipole and second-order quadrupole interactions and is consistent with the same 9700 K activation energy as T_1^{-1}. This shows that the same motions that give rise to T_1^{-1} for $T > 500$ K occur at a slower rate down to at least $T = 390$ K. At higher temperatures $T_{1\rho}^{-1}$ attains a plateau value and does not decrease as expected in spin-1/2 systems.[21] We believe this reflects contributions of the noncentral levels to the observed relaxation. At higher temperatures (> 550 K) $T_{1\rho}^{-1}$ is apparently limited by $\sim 10\ T_1^{-1}$ and again increases. We can offer no explanation for the factor of 10.

A map of the ^{23}Na relaxation data is shown in Fig. 7. The symbols on the figure are taken from the onset of line narrowing in the high-field $(T_2^*)^{-1}$ data, the motional broadening peak in the low-field T_2^{-1} data, and the peak in the low-field T_1^{-1} results. The relaxation map shows that all of the ^{23}Na relaxation data can be explained by a single thermally activated motion,

$$\omega_D = \omega_D(\infty)\exp\left(-\frac{E_a}{k_BT}\right), \quad (7)$$

with the parameters $E_a/k_B = 9700$ K (the energy that describes the T_1^{-1} data) and $\omega_D(\infty) = 1.7 \times 10^{14}$ s^{-1}.

Although the emphasis of this study has been on β-NaSn, some measurements on α-NaSn were made. Figure 5 shows that the ^{23}Na T_1^{-1} is frequency independent, demonstrating that the Na motion is fast [$\omega_D = \tau_D^{-1} \gg \omega_0$; see Eq. (4)]. Thus we have $\omega_D \gg 10^9$ s^{-1} in α-NaSn. *Assuming* ω_Q^2 to be the same as in β-NaSn and assuming the relaxation is entirely quadrupolar, the observed value of T_1^{-1} yields $\omega_D = 4.4 \times 10^{11}$ s^{-1}, from Eq. (4). This estimate of ω_D is comparable to the 1.9×10^{11} s^{-1} obtained from neutron scattering data.[5] The discrepancy suggests that ω_Q in α-NaSn may *not* be the same as in β-NaSn and/or the discrepancy may point to the different definitions of correlation rate in the models employed. ^{23}Na line shapes in α-NaSn are very narrow (~ 700 Hz FWHM) and display very little structure, indicating that motions are very rapid in the α phase and nearly completely average the second-order nuclear quadrupole interaction of the central transition. We did not attempt to detect the ^{23}Na satellites in the α phase.

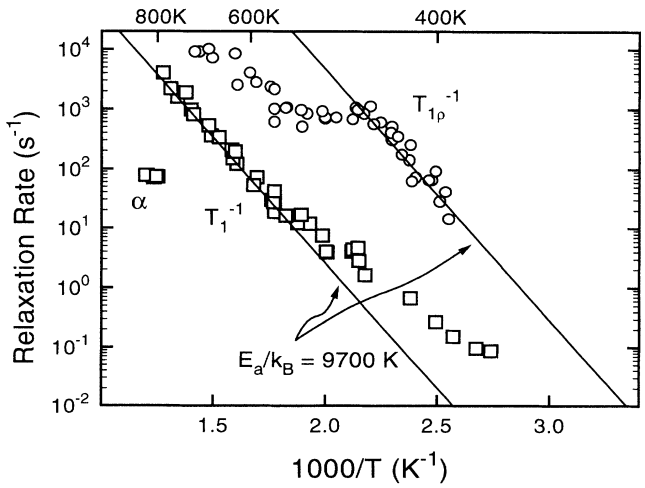

FIG. 6. ^{23}Na rotating-frame spin-lattice relaxation rate $T_{1\rho}^{-1}$ as a function of reciprocal temperature, shown as circles. $T_{1\rho}$ was measured at 8 T and $\gamma H_1/2\pi = 13.1$ kHz. At low temperatures, $T_{1\rho}^{-1}$ displays the same 9700 K activation energy seen in T_1^{-1} at higher temperatures. High-field T_1^{-1} data are shown for comparison (squares).

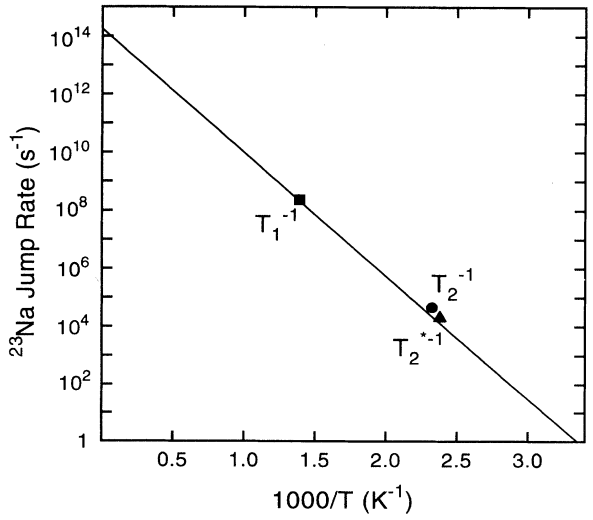

FIG. 7. ^{23}Na relaxation map. Na jump rates obtained from the low-field T_1^{-1} maximum (solid square), low-field T_2^{-1} peak (solid circle), and high-field T_2^{*-1} (solid triangle) are shown. The solid line obtained from T_1^{-1} data shows that the sodium relaxation data can be explained by a single activated motion with $E_a/k_B = 9700$ K and $\omega_D(\infty) = 1.7 \times 10^{14}$ s^{-1}.

C. Sn motions

The temperature evolution of the ^{119}Sn ($I = 1/2$) line shape is shown in Fig. 8. At room temperature the broad (105 kHz) Sn line shape is characteristic of a chemical shift anisotropy powder pattern (some distortion is evident and is due to incomplete spectral coverage by the rf pulses). The powder pattern is not uniaxially symmetric indicating that the Sn_4 tetrahedra or their environments are distorted. The deviations from exact tetrahedral units are also evident in interatomic distances determined by x rays.[1] At high temperatures the ^{119}Sn resonance line narrows as a result of Sn motion, either reorientation of the Sn_4 tetrahedra or Sn diffusion. In order to investigate the nature and rate of the Sn motions, two-pulse spin echo and three-pulse stimulated-echo experiments were performed on β-NaSn, the results of which are shown in Fig. 9.

Spin echoes (90°-τ-180°-τ-echo) yield a direct measure of the Sn motion provided the motion rate ω_R (R for reorientations, see below) is much less than the static linewidth.[15,18] Because of the anisotropic chemical shift, a ^{119}Sn spin changes NMR frequency due to reorientations of the Sn_4 units or hopping between tetrahedra. If the spin changes NMR frequency between the initial rf pulse and the occurrence of the spin-echo, the spin will be strongly dephased (phase error $\Delta\phi \gg 1$). Thus, only

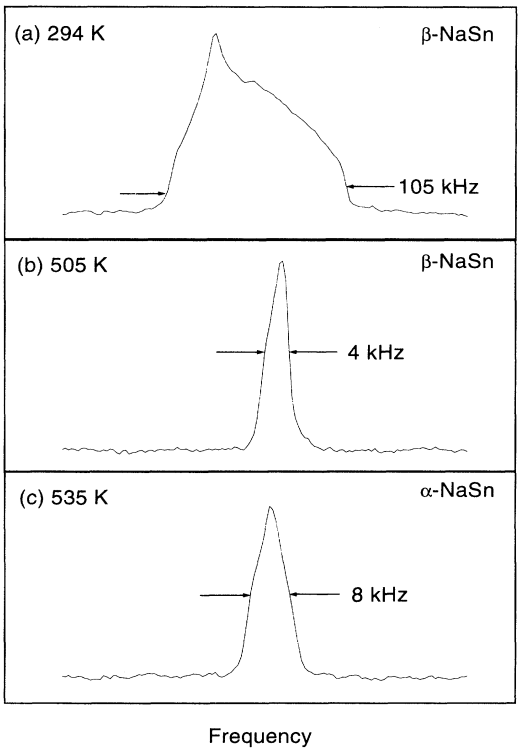

FIG. 8. ^{119}Sn NMR spectra of NaSn at high-field (126.9 MHz) at three temperatures. Line narrowing due to Sn motions is evident in (b). Structure in the α-NaSn spectrum at 535 K shows that the time averaged Sn environment is not cubic. Note that the three frequency scales are different.

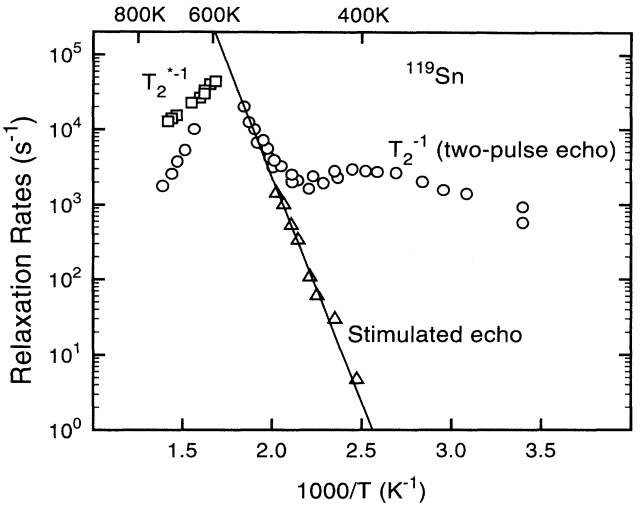

FIG. 9. Relaxation rates of ^{119}Sn in β-NaSn. The circles are T_2^{-1} from spin echoes; T_2^{-1} is nearly independent of temperature below 440 K due to dipolar coupling. The squares are $(T_2^*)^{-1}$ from the FID at high temperatures. Stimulated-echo data are shown as triangles. The line is a fit to the data and corresponds to an activation energy of 13 800 K. The stimulated-echo and T_2^{-1} data extend over four decades in rate.

^{119}Sn spins which have never jumped during the time 2τ contribute to the echo; the echo amplitude decays as $\exp(-2\tau/T_2)$, with $T_2^{-1} = \omega_R$. At low temperatures the dipole interaction will contribute to the observed T_2^{-1} so that $T_2^{-1} \neq \omega_R$, as in Eq. (1). The T_2^{-1} data in Fig. 9 show that at low temperatures T_2^{-1} is nearly temperature independent and of the magnitude expected for dipole interactions. The rapid increase in T_2^{-1} at high temperatures indicates T_2^{-1} is determined by Sn motions; thus in this region $T_2^{-1} = \omega_R$. Because the high-temperature T_2^{-1} data extend only over one decade due to the dipolar background, an accurate activation energy cannot be extracted from T_2^{-1} alone.

In order to measure slower rates of Sn motion we used the stimulated-echo (90°-τ-90°-t-90°-τ-echo) sequence.[19] The initial 90° pulse rotates the magnetization into the transverse plane where it is allowed to precess for a time τ (dephasing time). The second 90° pulse stores the magnetization along the z axis, followed by a waiting time t. The magnetization is then inspected by rotating it into the transverse plane again with a third 90° pulse; the remaining magnetization forms a stimulated echo at time τ (rephasing time) after the third 90° pulse. In the limit $\omega_R\tau \ll 1$, the Sn atoms have a negligible probability of reorienting during time τ, i.e., all Sn frequency changes occur during the longer time interval t. During the waiting interval t the magnetization is stored along the static field, so spin precession is not relevant. If any spin jumps during the waiting time t such that its Larmor frequencies during the dephasing and rephasing times are different, it will not contribute to the stimulated echo (phase error $\Delta\phi \gg 1$, the strong collision limit).

The ^{119}Sn stimulated-echo amplitude as a function of time t at the temperatures 444 K and 494 K is displayed in Fig. 10. The figure shows that the magnetization decays from its initial value to a baseline which is nearly 1/4 of the initial magnetization. This is precisely the behavior expected if the Sn motion is reorientation of the Sn_4 tetrahedra. The 1/4 baseline is due to the fact that there are four Sn sites (with their four associated frequencies) on any Sn_4 tetrahedron. If the echo decay is due to reorientations of the tetrahedra, then when $\omega_R t \gg 1$ there is a 1-in-4 chance that a Sn atom has returned to the same position (and NMR frequency) that it started with.[22] If the Sn atom has returned to its original frequency then it still contributes fully to the echo. Hence the baseline of 1/4 is expected for Sn reorientations. The 32 Sn sites per unit cell in β-NaSn are grouped into 8 tetrahedra, which are divided into two groups of four tetrahedra related by translational or inversion symmetry. Thus, any crystallite has eight Sn frequencies and a baseline of 1/8 would be expected for the stimulated echo for Sn diffusion. The stimulated-echo data therefore confirm that the Sn motion is reorientation of intact, nonexchanging Sn_4 tetrahedra. Both the stimulated-echo and high-temperature T_2^{-1} data are in the strong collision limit so both decay rates equal ω_R, the reorientation rate for the Sn_4 tetrahedra. The solid line in Fig. 9 is fitted to the two-pulse and three-pulse echo data and shows that the Sn_4 reorientations are thermally activated with $E_a/k_B = 13\,800$ K and $\omega_R(\infty) = 2.3 \times 10^{15}$ s^{-1}. We cannot rule out exchange of Sn atoms between different tetrahedra at a rate much slower than the reorientations.

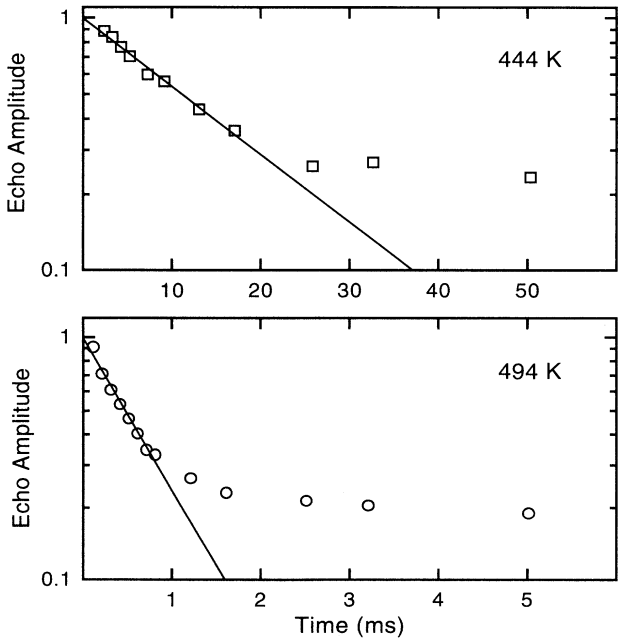

FIG. 10. Stimulated (three-pulse) echo amplitude as a function of delay time between second and third pulses for ^{119}Sn at 444 K and 494 K. The amplitude decays at long times to nearly 25% of the initial amplitude. This confirms that the Sn nuclei jump between four discrete frequencies, demonstrating that the Sn motion is tetrahedral reorientation. The lines fit the initial portions of the decays.

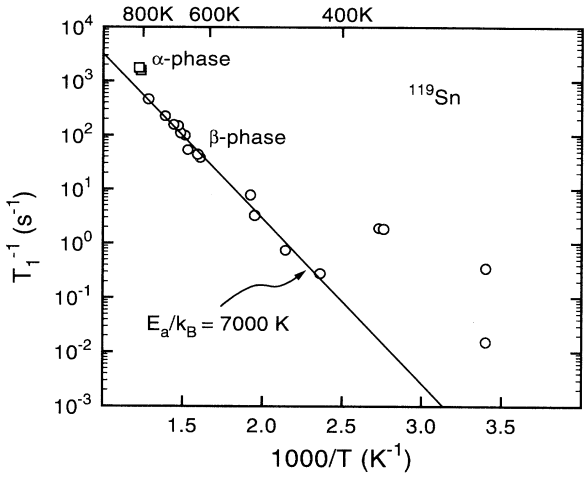

FIG. 11. High-field (8.0 T) ^{119}Sn spin-lattice relaxation rate T_1^{-1} as a function of reciprocal temperature. Relaxation rates for β-NaSn are given by circles, α-NaSn by squares. The line drawn is a fit to the β-NaSn data and represents an activation energy of 7000 K. The scatter in the low-temperature T_1^{-1} data reflects the differing amounts of impurities.

The ^{119}Sn T_1^{-1} as a function of temperature is shown in Fig. 11. T_1^{-1} in the β phase displays a thermally activated relaxation mechanism at high temperatures with an activation energy of 7000 K, substantially less than the activation energy for Sn_4 reorientations. The room temperature ^{119}Sn T_1^{-1} values varied as the samples were exposed to high temperatures (see scatter in Fig. 11), but the high temperature T_1^{-1} remained the same. Because this is similar to the ^{23}Na T_1^{-1}, we believe that the room temperature ^{119}Sn relaxation is also due to impurities. For relaxation due to motional modulation of chemical shift anisotropy, Abragam[20] gives the relaxation rate

$$\frac{1}{T_1} = \frac{3}{10}(\Delta\omega)^2\left(1+\frac{\eta^2}{3}\right)\left(\frac{\tau_R}{1+\omega_0^2\tau_R^2}\right) \tag{8}$$

which has a maximum at $\omega_0\tau_R = 1$. Here $\Delta\omega$ describes the frequency shift associated with the *largest element* of the traceless chemical shift anisotropy tensor. For $\omega_0\tau_R = 1$, Eq. (8) reduces to

$$\left(\frac{1}{T_1}\right)_{\max} = \frac{3}{20}\frac{(\Delta\omega)^2}{\omega_0}\left(1+\frac{\eta^2}{3}\right). \tag{9}$$

Approximating $\eta = 0$ (the largest possible error is 33%), $\Delta\omega$ equals 2/3 of the overall room temperature linewidth (i.e., $\Delta\omega = 4.4\times10^5$ s^{-1}) and $(T_1^{-1})_{\max} \sim 40$ s^{-1}. This is an order of magnitude smaller than the largest observed $T_1^{-1} = 500$ s^{-1}. Furthermore, the above estimate is for the *maximum* rate, predicted for $\omega_R = \omega_0$. But using the reorientation parameters $\omega_R(\infty)$ and E_a/k_B reported above, the calculated reorientation rate at $T_{\alpha\beta}$ in the β phase is only 2.7×10^7 s^{-1}, a factor of 30 smaller than ω_0.

From Eq. (8), the predicted T_1^{-1} is 2.5 s^{-1}, two orders of magnitude smaller than the observed ^{119}Sn relaxation. Thus modulation of the chemical shift anisotropy is not capable of generating the observed ^{119}Sn relaxation. The mechanism likely to be responsible for this strong T_1^{-1} relaxation is electrons and holes generated by thermal excitation in the semiconductor. The calculated band gap[2,23] for NaSn is 0.3 eV = 3240 K, which would lead us to expect a smaller activation energy (essentially half the band gap) than observed for the Sn relaxation. Impurities or deviations from 1:1 stoichiometry that act as dopants are expected to result in an activation energy *smaller* than the intrinsic value. We were unable to detect a temperature-dependent Knight shift (within a sensitivity of 30 kHz) that would arise from the thermally generated carriers. By comparison with the shift and relaxation of Sn metal (Korringa relation),[24] the T_1^{-1} observed in β-NaSn at $T_{\alpha\beta}$ would require a shift of 140 kHz, in a delocalized electron model. Fixed paramagnetic centers remain a possible explanation of the observed T_1^{-1}. A second possibility is enhanced relaxation by conduction electrons (compared to the Knight shift) which has been described for disordered conductors.[25]

Figure 8 shows an α-phase ^{119}Sn line shape obtained at 535 K. The structure evident in the spectrum shows that, even averaged over the time scale of 10^{-4} s set by the linewidth, the Sn sites do not have cubic symmetry. This supports the neutron scattering data which indicate that the α phase possesses a triclinic structure.[5]

IV. CONCLUSIONS

Diffusion of Na^+ cations and reorientations of $(Sn_4)^{4-}$ anions occur in β-NaSn. The rates and activation energies of the two motions are different, indicating that the two motions are not directly correlated. Na motion, evident in ^{23}Na T_1^{-1}, T_2^{-1}, $T_{1\rho}^{-1}$, and T_2^{*-1} NMR measurements, is described by E_a/k_B = 9700 K and $\omega_D(\infty) = 1.7 \times 10^{14}$ s^{-1}. Sn motions, evident in ^{119}Sn T_2, line shape, and stimulated-echo NMR experiments are described by E_a/k_B = 13 800 K and $\omega_R(\infty) = 2.3 \times 10^{15}$ s^{-1}. The baseline of 1/4 in the stimulated-echo data shows that the Sn motion is reorientation of the $(Sn_4)^{4-}$ tetrahedra and not Sn hopping between tetrahedra.

Sn T_1^{-1} relaxation is also thermally activated, with E_a/k_B = 7000 K, substantially smaller than the energy for reorientation. Furthermore, the observed maximum rate is too large to be explained by motional modulation of the chemical shift anisotropy. The Sn T_1^{-1} mechanism is not fully understood, but is believed to be due to thermally activated carriers.

ACKNOWLEDGMENTS

The authors appreciate the assistance of Ken Tasaki with software for visualization of the β-NaSn structure. We thank N. L. Adolphi for the construction of the furnace for the high-field measurements. The assistance of W. E. Buhro and J. Haase is gratefully acknowledged. We thank A. J. Vega for informing us of Ref. 19. The research at Washington University was supported through NSF Grants No. DMR 90-24502 and No. 94-03667. The work at Argonne was supported by the Department of Energy, Division of Materials Science, Office of Basic Energy Sciences through Contract No W-31-109-ENG-38. A. F. McDowell was supported by the Midstates Pew Mathematics and Science Consortium, funded by a grant from the Pew Charitable Trusts.

[1] W. Müller and K. Volk, Z. Naturforsch. Teil B **32**, 709 (1977).
[2] F. Springlekamp, R. A. de Groot, W. Geertsma, W. van der Lugt, and F. M. Mueller, Phys. Rev. B **32**, 2319 (1985).
[3] M.-L. Saboungi and D. L. Price, J. Non-Cryst. Solids **150**, 260 (1992).
[4] H. Schäfer, B. Eisenmann, and W. Müller, Angew. Chem **12**, 694 (1973).
[5] M.-L. Saboungi, J. Fortner, W. S. Howells, and D. L. Price, Nature **365**, 237 (1993).
[6] W. Hume-Rothery, J. Chem. Soc. **131**, 947 (1928).
[7] M.-L. Saboungi, G. K. Johnson, and D. L. Price, in *Statics and Dynamics of Alloy Phase Transformations*, edited by P. E. A. Turchi and A. Gonis (Plenum, New York, 1994).
[8] B. P. Alblas, W. van der Lugt, J. Dijkstra, W. Geertsma, and C. van Dijk, J. Phys. F **13**, 2465 (1983).
[9] C. van der Marel, A. B. van Oosten, W. Geertsma, and W. van der Lugt, J. Phys. F **12**, 2349 (1982).
[10] L. Börjesson and L. M. Torell, Phys. Rev. B **32**, 2471 (1985).
[11] M. S. Conradi, Concepts Magn. Reson. **5**, 243 (1993).
[12] R. A. McKay, U.S. Patent No. 4,446,431 (1 May 1984).
[13] E. Fukushima and S. B. W. Roeder, *Experimental Pulse NMR* (Addison-Wesley, Reading, MA, 1981).
[14] M. H. Cohen and F. Reif, in *Solid State Physics: Advances in Research and Applications*, edited by F. Seitz and D. Turnbull (Academic, New York, 1957), Vol. 5.
[15] C. P. Slichter, *Principles of Magnetic Resonance* (Springer-Verlag, New York, 1990).
[16] D. Freude and J. Haase, in *NMR Basic Principles and Progress*, edited by P. Diehl, E. Fluck, H. Gunther, R. Kosfeld, and J. Seelig (Springer-Verlag, Berlin, 1993), Vol. 29.
[17] N. Boden, in *The Plastically Crystalline State*, edited by J. N. Sherwood (Wiley, New York, 1979).
[18] J. A. Pople, W. G. Schneider, and H. J. Bernstein, *High-Resolution Nuclear Magnetic Resonance* (McGraw-Hill, New York, 1959).
[19] A. Baram, Z. Luz, and S. Alexander, J. Chem. Phys. **58**, 4558 (1973).
[20] A. Abragam, *The Principles of Nuclear Magnetism* (Clarendon, Oxford, 1961).
[21] D. C. Ailion, in *Advances in Magnetic Resonance*, edited by J. S. Waugh (Academic, New York, 1971), Vol. 5.
[22] S.-B. Liu and M. S. Conradi, Phys. Rev. B **30**, 24 (1984).
[23] J. A. Meijer, Ph.D. thesis, University of Groningen, 1988.
[24] W. P. Knight, in *Solid State Physics: Advances in Research and Applications*, edited by F. Seitz and D. Turnbull (Academic, New York, 1956), Vol. 2.
[25] W. W. Warren, Phys. Rev. B **3**, 3708 (1971).